Biosensors and Bioelectronics 25 (2010) 1186–1192

Contents lists available at ScienceDirect

Biosensors and Bioelectronics

journal homepage: www.elsevier.com/locate/bios

Al^{3+}-directed self-assembly and their electrochemistry properties of three-dimensional dendriform horseradish peroxidase/polyacrylamide/platinum/single-walled carbon nanotube composite film

Jingsi Xie[a], Xiumei Feng[a], Jianqiang Hu[a,**], Xiaohua Chen[a], Aiqing Li[b,*]

[a] College of Chemistry and Chemical Engineering, South China University of Technology, Guangzhou 510640, PR China
[b] College of Medicine & Public Health, The Ohio State University, Columbus, OH 43210, USA

ARTICLE INFO

Article history:
Received 19 August 2009
Received in revised form
30 September 2009
Accepted 8 October 2009
Available online 6 November 2009

Keywords:
Direct electrochemistry
Electrocatalysis
Pt/SWCNT heterojunction
Horseradish peroxidase
Al^{3+}-directed PAM self-assembly
Biosensor

ABSTRACT

A novel general methodology for protein immobilization and third-generation biosensor construction is demonstrated, which involves Al^{3+}-directed polyacrylamide (PAM) self-assembly into an ordered dendriform structure, easily immobilizing enzymes and nanoparticles. Platinum/single-walled carbon nanotube (Pt/SWCNT) heterojunction nanomaterials were for the first time fabricated via an EDTA-directed synthesis strategy. The Pt/SWCNTs were employed as a supporting matrix to explore a novel immobilization and biosensing platform of redox proteins through cooperating Al^{3+}-directed PAM self-assembly. Compared with the almost single-layer horseradish peroxidase (HRP)/PAM film electrode, multilayer HRP/PAM/Pt/SWCNT film electrode exhibited a pair of much stronger redox peaks at −0.22 V (vs. Ag/AgCl). Moreover, with advantages of the ordered multilayer HRP/PAM/Pt/SWCNT film, facilitated direct electron transfer of the metalloenzymes with an apparent heterogeneous electron transfer rate constant (k_s) of $14.94 \pm 1.36\ s^{-1}$ and smaller peak-to-peak separation (ΔE_p) of about 37 mV was acquired on the PAM/Pt/SWCNT-based enzyme electrode. The PAM/Pt/SWCNT-based biosensor demonstrated significant electrocatalytic activity for the reduction of hydrogen peroxide with a small apparent Michaelis–Menten constant (87 μM), wide linear range (1–270 μM), very low detection limit (0.08 μM, $S/N = 3$), and high sensitivity ($372\ mA\ cm^{-2}\ M^{-1}$). Together, these indicated that the Al^{3+}-directed HRP/PAM/Pt/SWCNT film was one of ideal candidate materials for direct electrochemistry of redox proteins and the construction of the related enzyme biosensors, and may find potential applications in biomedical, food, and environmental analysis and detection.

1. Introduction

Direct electrochemistry and electrocatalysis of redox proteins constructed on nanomaterials have recently attracted considerable attention because it can not only serve as an ideal model to understand the kinetics and thermodynamics of biological redox processes (Armstrong et al., 1988; Zhao et al., 2008), but also offer great potential for applications in many fields such as the construction of third-generation biosensors (Cao et al., 2008), the detection of bacterial cells (Varshney and Li, 2009), bioelectronic devices (Arya et al., 2009), biocatalysis (Zhang et al., 2007), biodetection (Pal et al., 2007), and protein identification (Li et al., 2007). However, it is difficult for proteins to realize direct electron transfer on "bare" electrodes because of their adsorptive denaturation, deeply embedded active centers, and often unfavorable orientations (Heller, 1990). To immobilize proteins and nanomaterials and further fabricate electrochemical biosensors using a cast method, it is usually essential to employ cross-linking agents, such as nafion, chitosan, ferrocene derivatives, and glutaraldehyde. However, the cross-linking utilization contains two fatal shortcomings for fabricating stable and high-performance biosensors: (i) it is difficult to form an ordered structure and thus obtain favorable protein orientations; (ii) these cross-linking agents, to some extent, restrain electron transfer between enzymes and underlying electrodes because they lengthen electron transfer path (Chen et al., 2009). Given this, it will be an amazing success to construct high-performance biosensors without using any cross-linking agents. In our latest work, we developed a combined hydrogen bond and electrostatic assembly strategy to successfully construct a stable and high-performance biosensor without any cross-linking agents, whose electron transfer capacity is 3.5-fold stronger than that from

* Corresponding author. Tel.: +1 614 292 4420; fax: +1 614 688 8742.
** Corresponding author. Tel.: +86 20 222 36670; fax: +86 20 222 36670.
E-mail addresses: jqhusc@scut.edu.cn (J. Hu), li.586@osu.edu (A. Li).

0956-5663/$ – see front matter © 2009 Elsevier B.V. All rights reserved.
doi:10.1016/j.bios.2009.10.007

the chitosan-constructed biosensor (Chen et al., 2009). Nevertheless, the self-assembly strategy is not still a general method because it is only suitable for nanomaterials containing copious oxygen atoms and the electrode used requires to be activated.

Polyacrylamide (PAM) is an important water-soluble polymer and an efficient flocculant, having a variety of applications including enhanced oil recovery (Li et al., 2009), wastewater treatment (Sanghi et al., 2006), and soil erosion control (Sojka et al., 2007). On its macromolecular chains, there are a great number of acetylamine groups. Many metal ions (e.g., Al^{3+}, Cr^{3+}) can easily make PAM cross-linking into an ordered film through the complexation of metal ion with the hydrolyzed carboxylate groups ($-COO^-$) of PAM (Montanari et al., 1994). Recently, polymerized PAM microgels as a supporting matrix have successfully been utilized to immobilize redox proteins and fabricate electrochemical biosensors (Perez et al., 2006). However, the polymerization process required relatively complicated operations and the polymerization for protein immobilization lowered the protein bioactivity to some degree (Lopez et al., 2007). Up to now, to the best of our knowledge, this is the first study showing that Al^{3+}-directed ordered self-assembly film is utilized to immobilize proteins and nanomaterials and construct electrochemical biosensors.

One-dimensional (1D) metal/semiconductor heterojunction nanomaterials are of particular importance because of their novel structures, unique electrical and optical properties, and central roles in fabricating electronic nanodevices (Xiang et al., 2006). Both platinum (Pt) and single-walled carbon nanotubes (SWCNTs) of the Pt/SWCNT heterojunctions possess excellent electron-conducting capacity (Tian et al., 2007; Bachtold et al., 2001), which, therefore, are reasonably expected to construct promising electrochemical biosensors. In the present work, we designed a new general method, i.e., Al^{3+}-directed PAM self-assembly, to immobilize proteins (e.g., horseradish peroxidase (HRP)) and nanoparticles (e.g., Pt/SWCNTs) and thus fabricate a very promising electrochemical biosensor. With the aid of the 3D ordered HRP/PAM/Pt/SWCNT composite film, HRP could well retain its native structure and bioactivity, and facilitated direct electron transfer of HRP entrapped in the self-assembly film has been acquired. Comparative studies revealed that relative to the biosensor based on HRP/PAM, the biosensor based on HRP/PAM/Pt/SWCNT had not only rather stronger direct electron transfer capacity but also displayed more excellent electrochemical performance over a wider linear range along with good stability and sensitivity for the detection of hydrogen peroxide. The ordered HRP/PAM/Pt/SWCNT composite film with copious pores of micrometer-scale sizes was proved to be a promising candidate for the construction of enzyme-based electrochemical biosensors. The data presented here may have greatly potential impact on the design and application of electrochemical biosensors.

2. Materials and methods

2.1. Chemicals and reagents

Horseradish peroxidase (HRP, >250 u mg^{-1}) was purchased from Yuanju Biology Science and Technology Co. Ltd. (Shanghai, China). Polyacrylamide (PAM, average molecular weight of about 3×10^6) came from Sinopharm Chemical Reagent Co. Ltd (Shanghai, China). Single-walled carbon nanotubes (SWCNTs, 95%) were obtained from Nanoport. Co. Ltd (Shenzhen, China) and sodium borohydride ($NaBH_4$, 99%) came from Aldrich. All other chemical reagents were obtained from Guangdong Guanghua Chemical Reagent Company. All the reagents were of analytical grade and used without further purification. All aqueous solutions were prepared with Milli-Q purified water (>18.0 MΩ cm). 20 mM phosphate buffer solution (PBS, pH 7.0) was prepared by mixing stock standard solutions of NaH_2PO_4 and Na_2HPO_4.

2.2. Apparatus and measurements

Scanning electron microscopy (SEM) was performed with a field-emission microscope (LEO, 1530 VP) operated at an accelerating voltage of 30 kV. Powder X-ray diffraction (XRD) pattern was recorded on a powder sample using a D/max-IIIA (Japan) X-ray diffractometer with Cu Kα radiation (λ = 0.15418 nm). UV–visible (UV–vis) absorption spectroscopy measurement was carried out with a U-3010 spectrophotometer (Hitachi, Japan). Fourier-transform infrared (FTIR) spectra were obtained on Tensor 27 (Bruker Company, German). Electrochemical impedance spectroscopy (EIS) spectra were acquired using an AUTOLAB advanced electrochemical system (Swiss). Electrochemical experiments were carried out at room temperature using a CHI 660 electrochemical workstation (CH Instruments, Inc., Austin, USA). All electrochemical measurements were based on a three-electrode system with the film electrode as working electrode, an Ag/AgCl (3 M KCl) electrode as reference electrode, and a platinum wire as auxiliary electrode, respectively. 20 mM pH 7.0 PBS was used as the electrolyte in all experiments.

2.3. Synthesis of Pt/SWCNT heterojunction nanomaterials

In a typical procedure for the synthesis of Pt/SWCNTs, SWCNTs were first purified through refluxing for 48 h in 2.6 M HNO_3 as described previously (Lin et al., 2002), and the complex compound of Pt-EDTA was prepared through refluxing the mixture solution containing 0.5 mM H_2PtCl_6, 2.5 mM NaOH, 3.8 mM EDTA, and 3.2 mM $Na_3C_6H_5O_7$ for 1 h. Then, the purified and dried SWCNTs (1 mg) were dispersed into the 30 mL as-prepared Pt-EDTA complex, and the mixture was placed in iced water for 10 min while stirring. Next, 1.0 mL of freshly prepared ice cold 0.10 M $NaBH_4$ solution was added to the ice-chilled mixture and kept stirring for 30 min when the reaction turned into brown. Finally, the Pt/SWCNT heterojunction nanomaterials were obtained through centrifuging at 2000 rpm and drying at 50 °C for 4 h. The whole synthesis route is illustrated in Fig. S1.

2.4. Preparation of different modified electrodes

3-mm-diameter glassy carbon (GC) electrode was first polished with alumina slurry of successively smaller particles (1.0, 0.3, and 0.05 μm diameters, respectively). Then, the electrode was cleaned by ultrasonication in ultrapure water and ethanol, respectively. To prepare Al^{3+}-directed HRP/PAM/Pt/SWCNT modified electrode, the PBS containing 1.0% PAM, 0.2 mg/mL Pt/SWCNTs, and 1.25 mg/mL HRP was first prepared. Then, 10 μL of the PBS was cast onto the surface of the cleaned GC electrode. Next, 5 μL of 8.0 mM $Al_2(SO_4)_3$ was added to the electrode. Finally, a uniform film electrode was formed through putting the as-prepared electrode overnight at room temperature, and then used for electrochemical investigations or stored at 4 °C.

For comparison, Al^{3+}-directed PAM/Pt/SWCNT/GC and Al^{3+}-directed HRP/PAM/GC electrodes were also prepared according to the same procedure.

3. Results and discussion

3.1. Morphology and structure characterization of the Pt/SWCNT heterojunctions and HRP/PAM/Pt/SWCNT composite film

Fig. 1A shows a typical TEM image of the as-prepared Pt/SWCNT heterojunctions. It can be clearly seen that Pt nanoparticles, hav-

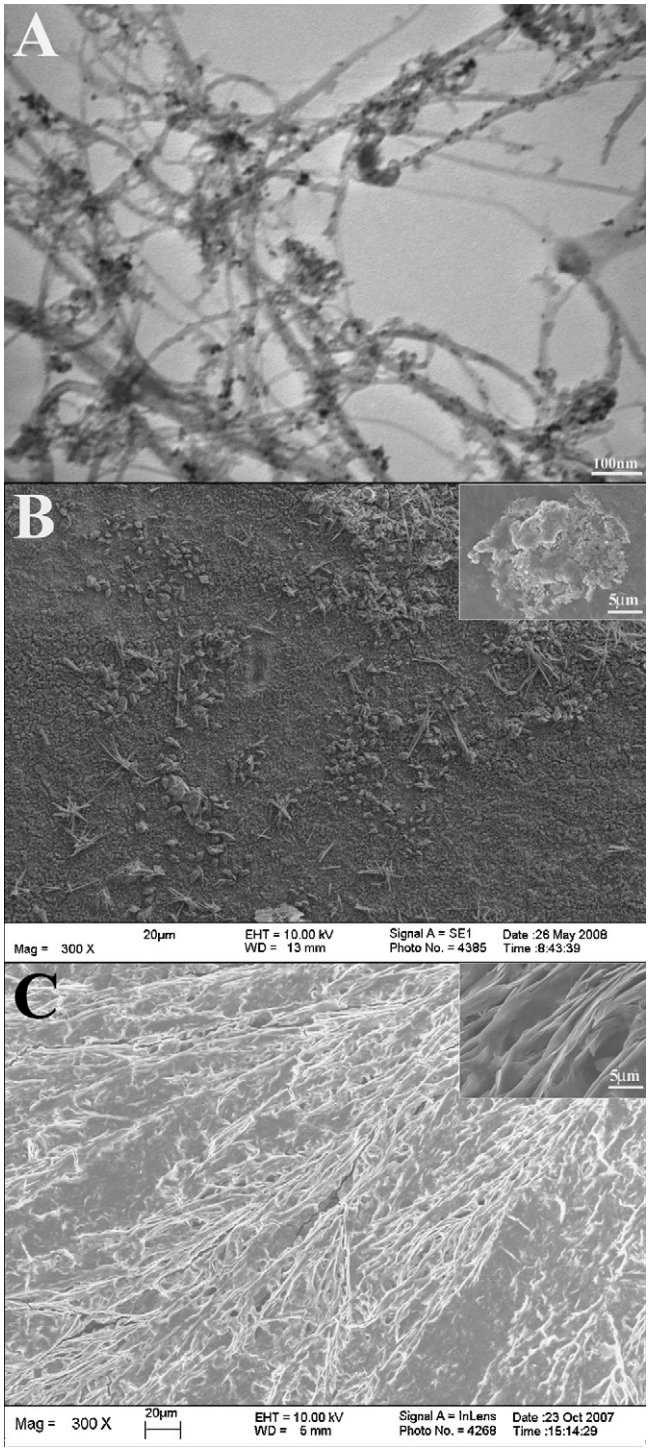

Fig. 1. (A) TEM image of EDTA-assisted Pt/SWCNT heterojunctions and (B and C) SEM images of HRP/PAM/Pt/SWCNT composite films prepared without or with Al^{3+}-directed self-assembly. Scale bar: (A) 100 nm and (B and C) 20 μm; inset: 5 μm.

ing the average diameter of approximately 11 nm, were partly or entirely entrapped into SWCNTs. To verify the components of the sample, XRD measurement was preformed. The (0 0 2) diffraction peak in Fig. S2 corresponded to graphite from the SWCNTs (JCPDS: 25-0284), which was consistent with the previous study (Wen et al., 2008). The diffraction peaks at $2\theta = 39.8^\circ$, 46.3°, 67.5°, and 81.3° could be indexed to (1 1 1), (2 0 0), (2 2 0), and (3 1 1) planes of a pure face-centered crystalline structure of Pt (JCPDS: 87-0646). The XRD results suggested that SWCNTs and Pt nanoparticles still retained their crystalline structures in the Pt/SWCNT heterojunctions, which was similar to the Au/MWCNT heterojunctions previously described (Feng et al., 2009).

Fig. 1C gives a representative SEM image of Al^{3+}-directed HRP/PAM/Pt/SWCNT self-assembly film. It possessed 3D dendriform structure and contained numerous micron-scale cavities (the inset of Fig. 1C). Such 3D dendriform structure not only offered rather high surface area but also had highly active sites, which were much useful for proteins to sequester in the cavities or bind on the surface. Surprisingly, without Al^{3+} inducement, HRP/PAM/Pt/SWCNT mixture solution would form disordered film (Fig. 1B and its inset), which could not be immobilized onto GC electrode. This indicated that Al^{3+} played a key role in the formation of 3D ordered and porous HRP/PAM/Pt/SWCNT composite film.

3.2. Al^{3+}-directed self-assembly and EIS analysis of HRP/PAM/Pt/SWCNT composite film

The 3D ordered HRP/PAM/Pt/SWCNT composite film on the polished GC electrode was acquired through the Al^{3+}-directed self-assembly process, as illustrated in Fig. 2. PAM and HRP PBSs were first introduced onto the GC electrode. Previous studies have demonstrated that metal ion easily coordinately bond with the hydrolyzed –COOH of PAM and form gelation (Cai and Huang, 2001). Consequently, when adding $Al_2(SO_4)_3$ PBS onto the as-prepared electrode, an ordered and uniform monolayer PAM/HRP/GC film was formed, which would be demonstrated by the following electrochemistry study. Interestingly, when $Al_2(SO_4)_3$ and Pt/SWCNT PBSs were introduced onto the electrode instead of $Al_2(SO_4)_3$ PBS, a 3D ordered multilayer HRP/PAM/Pt/SWCNT film was obtained. This was probably because the Pt atoms of the Pt/SWCNTs participated in the formation of the coordinate bond among $Al_2(SO_4)_3$, Pt/SWCNT, and PAM.

To evaluate the Al^{3+}-directed self-assembly process and interfacial electron transfer property of the HRP/PAM/Pt/SWCNT modified electrode, EIS was preformed. Previous studies have proved that the impedance spectrum involving a semicircle portion at high frequencies corresponds to the electron transfer limiting process (Pei et al., 2001), using which electron transfer resistance (Rct) can be gained by measuring the diameter. At the bare GC electrode (curve a in Fig. S3), the Rct could be estimated to be about 190 Ω. When PAM was assembled on the GC electrode surface by Al^{3+} inducement, its Rct was about 980 Ω (curve c in Fig. S3). Nevertheless, when entrapping the Pt/SWCNTs into the Al^{3+}-directed PAM film, the Rct (630 Ω, curve b in Fig. S3) decreased, suggesting that the Pt/SWCNT heterojunctions have good ionic conductivity and effectively facilitate electron transfer of the ferricyanide toward the electrode surface. However, a significant increase of the interfacial resistance (about 1800 Ω, curve e in Fig. S3) was observed when HRP was immobilized onto the GC electrode with the Al^{3+}-directed PAM, indicating that HRP hindering electron transfer pathway was successfully immobilized on the electrode surface (Wang et al., 2008). Nevertheless, the Rct (about 1290 Ω, curve d in Fig. S3) at the Al^{3+}-directed HRP/PAM/Pt/SWCNT/GC electrode decreased again relative to that at the Al^{3+}-directed HRP/PAM/GC electrode, further demonstrating that the Pt/SWCNT heterojunctions were rather helpful to speed up electron transfer between the underlying electrode and the electrolyte.

3.3. UV–vis spectroscopic characterization of HRP/PAM/Pt/SWCNT composite film

UV–vis spectroscopy is an effective means to probe possible denaturation of heme proteins because it can monitor possible changes of the Soret absorption band in the heme group (Xiao et al., 2009). Fig. 3 shows UV–vis absorption spectra of dry HRP, and

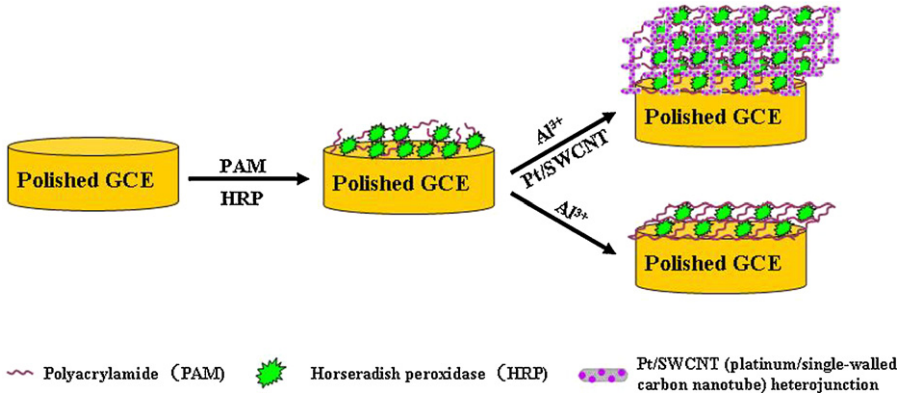

Fig. 2. Schematic illustration of the Al^{3+}-directed self-assembly of the HRP, PAM, and Pt/SWCNTs on the polished GC electrode.

Al^{3+}-directed PAM/Pt/SWCNT, HRP/PAM, and HRP/PAM/Pt/SWCNT films. Compared with dry Al^{3+}-directed PAM/Pt/SWCNT film (no characteristic peak, curve a), an obvious UV–vis absorption peak at around 405 nm from dry HRP film could be clearly discerned, which was a characteristic Soret absorption band of HRP (curve b). When HRP was entrapped in the Al^{3+}-directed PAM and PAM/Pt/SWCNT films, the positions and intensities of the HRP spectrum peaks were similar to that of pure HRP film (curves c and d), suggesting that the HRP still retained the essential feature of its native secondary structure in the Al^{3+}-directed PAM and PAM/Pt/SWCNT composite films and had good biocompatibility with PAM and Pt/SWCNTs. The good biocompability of HRP entrapped in the Al^{3+}-directed PAM and PAM/Pt/SWCNT films could perhaps be attributed to their rigid framework and high chemical activity, which were available to hide or bind HRP and thus restrained its conformational change and unfolding.

3.4. Direct electrochemistry of the film electrodes

Fig. 4A shows cyclic voltammograms of different modified electrodes in PBS at 0.1 V/s. No peak was observed (curve a) at the Al^{3+}-directed PAM/Pt/SWCNT electrode, showing that the PAM and Pt/SWCNTs were not electroactive materials in the potential range. However, the Al^{3+}-directed HRP/PAM electrode exhibited a couple of nearly reversible and well-defined peaks (curve b), which could be attributed to direct electron transfer between the HRP and the underlying electrode (Kafi et al., 2008). The apparent formal potential $E^{\circ\prime}$ estimated by $(E_{p,a}+E_{p,c})/2$ was about −0.23 V, where $E_{p,a}$ and $E_{p,c}$ are the anodic and cathodic peak potentials, respectively. The $E^{\circ\prime}$ was very close to that (−0.22 V) of native HRP in solution (Jia et al., 2005), further suggesting that PAM had excellent biocompability with HRP molecules. Using Faraday's law, $Q = nFA\Gamma^*$ (Q, n, F, A, and Γ^* represent the quantity of charge, the number of electron transferred, Faraday constant, effective electrode

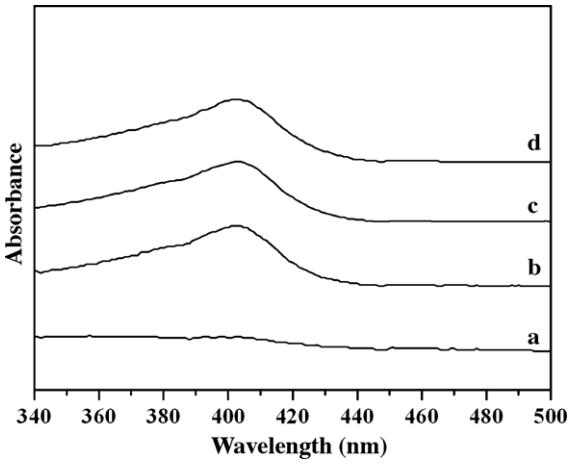

Fig. 3. UV–vis spectra of dry (a) Al^{3+}-directed PAM/Pt/SWCNT, (b) HRP, (c) Al^{3+}-directed HRP/PAM, and (d) Al^{3+}-directed HRP/PAM/Pt/SWCNT films.

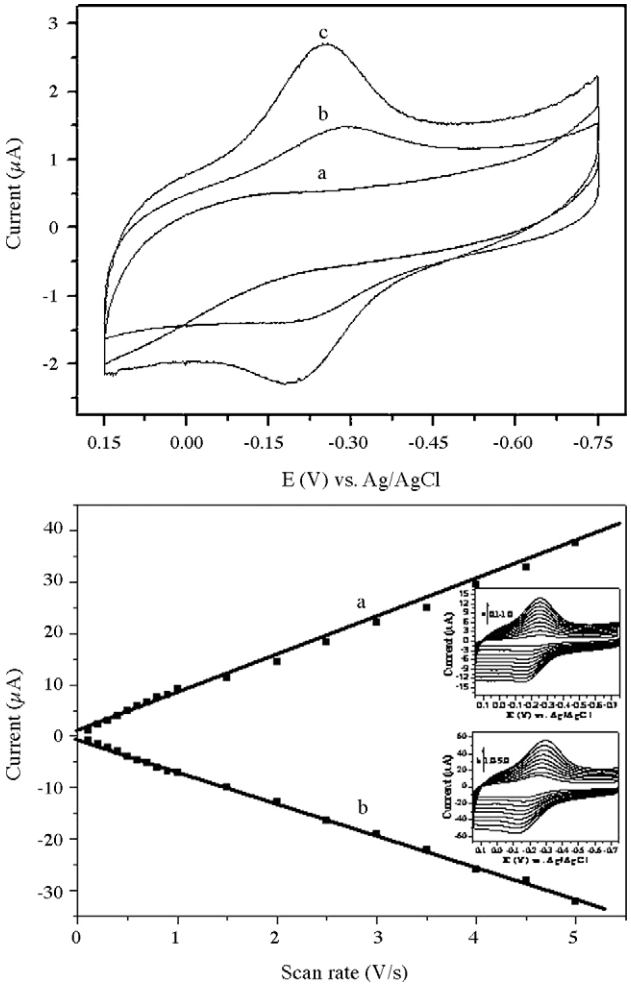

Fig. 4. (A) Cyclic voltammograms of (a) Al^{3+}-directed PAM/Pt/SWCNT/GC, (b) Al^{3+}-directed HRP/PAM/GC, and (c) Al^{3+}-directed HRP/PAM/Pt/SWCNT/GC electrodes in PBS with the scan rate of 0.1 V/s. (B) Plots of oxidation peak currents and reduction peak currents vs. scan rates for the Al^{3+}-directed HRP/PAM/Pt/SWCNT/GC electrode. Scan rates: 0.1, 0.2, 0.3, 0.4, 0.5, 0.6, 0.7, 0.8, 0.9, 1.0 V/s (inset a) and 1.0, 1.5, 2.0, 2.5, 3.0, 3.5, 4.0, 4.5, 5.0 V/s (inset b).

area, and surface average concentration of electroactive enzyme, respectively), the Γ^* of the electroactive HRP in the PAM film was estimated to be about 2.53×10^{-11} mol/cm^2 (assuming a one-electron transfer reaction), which was almost similar to that of the theoretical monolayer coverage (1.89×10^{-11} mol/cm^2) (Huang et al., 2002). Only nearly 0.57% of the total amount of adsorbed HRP (Γ, about 4.42×10^{-9} mol/cm^2) was deposited on the PAM/GC electrode, indicating the presence of a monolayer of electroactive HRP on the electrode surface.

Interestingly, when the Pt/SWCNT heterojunctions were introduced into the Al^{3+}-directed HRP/PAM composite system, the redox peak currents of the Al^{3+}-directed HRP/PAM/Pt/SWCNT electrode were significantly enhanced (curve c). The great enhancement indicated that the Pt/SWCNTs could greatly facilitate electron transfer between the HRP and the underlying electrode. The $E^{\circ\prime}$ of the redox peaks at the Al^{3+}-directed HRP/PAM/Pt/SWCNT electrode was estimated to be about −0.22 V, which was almost the same as that of native HRP in solution. The nearly same $E^{\circ\prime}$ disclosed that almost all HRP molecules entrapped in the Al^{3+}-directed PAM/Pt/SWCNT composite film could preserve their native structure (Jia et al., 2005). According to the formula $Q = nFA\Gamma^*$, the Γ^* of the electroactive HRP in the PAM/Pt/SWCNT film was estimated to be about 2.33×10^{-10} mol/cm^2 and the electroactive HRP in the PAM/Pt/SWCNT film was about 5.27% of the total HRP content deposited on the electrode, which was 12 times higher than that of the theoretical monolayer coverage and 9 times higher than that of the PAM film. This suggested that 12 layers of the self-assembly HRP molecules closest to the electrode participated in transferring electrons to the underlying electrode. The peak-to-peak separation (ΔE_p) was about 37 mV at 0.1 V/s, which was much smaller than that (74 mV) of the HRP in the PAM at the same scan rate. Such a smaller ΔE_p value revealed a rather fast electron transfer process. The excellent electrochemical properties could be ascribed to the following advantages. First, PAM, Pt, and SWCNT were all good electron transfer carriers. Second, the ordered multilayer self-assembly structure generated numerous micrometer-scale cavities and highly active sites, which may be available to bind HRP and provide an efficient electron-conducting tunnel. Finally, the ordered self-assembly film, serving as a rigid framework, could hide HRP and thus restrained its conformational change and unfolding for favoring the appropriate conformation.

Fig. 4B gives representative cyclic voltammograms of the Al^{3+}-directed HRP/PAM/Pt/SWCNT electrode scanned at low and high scan rates, respectively. It can be seen that both the reduction and oxidation peak currents increased linearly with increasing scan rates from 0.1 to 5.0 V/s, which demonstrated a surface-controlled process (Murray, 1984). The correlation coefficient, very close to the theoretical slope of 1 for thin layer voltammetry (Murray, 1984), indicated that almost all electroactive HRP-Fe(III) in the film were reduced on the forwarded cathodic scan and the reduced HRP-Fe(II) was then converted to the oxidized form (HRP-Fe(III)) on the reverse anodic scan. Thus, the Al^{3+}-directed PAM/Pt/SWCNT system provided a friendly microenvironment for the intercalated HRP to maintain its bioactivity and the Al^{3+}-directed HRP/PAM/Pt/SWCNT film underwent a reversible, fast, and surface-controlled electron transfer. The kinetic parameter k_s of the HRP immobilized on the Al^{3+}-directed PAM/Pt/SWCNT film was estimated using the model of Laviron (1974):

$$\log\frac{k_s}{s^{-1}} = \alpha\log(1-\alpha) + (1-\alpha)\log\alpha - \log\left[\left(\frac{RT/nF\upsilon}{s}\right)\right] - \frac{\alpha(1-\alpha)nF\Delta E_p}{2.3RT}$$

where α, k_s, ΔE_p, n, R, T, and υ mean charge transfer coefficient, heterogeneous electron transfer rate constant, peak separation, the number of electrons transferred, gas constant, absolute temperature, and scan rate, respectively. By taking α as 0.5 and $\upsilon > 0.2$ V/s, the average k_s was determined to be $14.94 \pm 1.36\ s^{-1}$, which was much larger than those at the reported zinc oxide nanorod ($1.15\ s^{-1}$) and clay–chitosan–gold nanoparticle nanocomposite ($2.95 \pm 0.20\ s^{-1}$) modified electrodes (Gu et al., 2009; Zhao et al., 2008). This implied that the HRP/PAM/Pt/SWCNT modified electrode facilitated more effectively electron transfer between the redox-active sites of enzyme and the electrode than other modified electrodes.

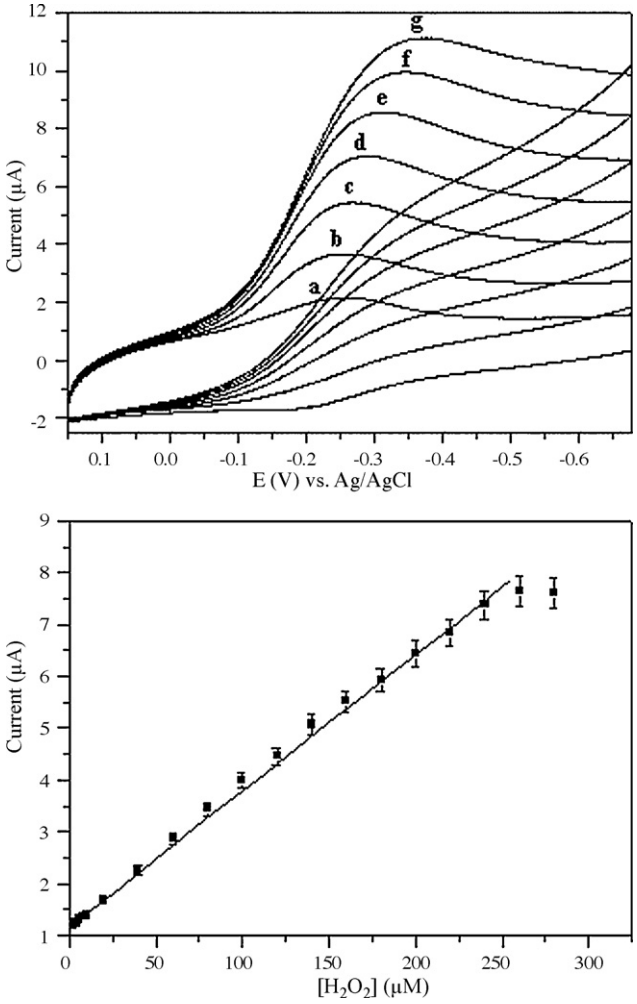

Fig. 5. (A) Bioelectrocatalysis of the biosensor towards H_2O_2 in PBS with the scan rate of 0.1 V/s and H_2O_2 concentrations of (a) 0, (b) 40, (c) 80, (d) 120, (e) 160, (f) 200, and (g) 240 μM. (B) Plot of electrocatalytic currents (I_{cat}) vs. H_2O_2 concentrations for the Al^{3+}-directed HRP/PAM/Pt/SWCNT electrode in PBS.

3.5. Electrocatalysis of the Al^{3+}-directed HRP/PAM/Pt/SWCNT/GC electrode

To evaluate the biocatalytical activity of HRP immobilized on the Al^{3+}-directed PAM/Pt/SWCNT modified electrode, the electrocatalytic property of the Al^{3+}-directed HRP/PAM/Pt/SWCNT/GC electrode toward H_2O_2 was investigated by cyclic voltammetry. Fig. 5A records cyclic voltammograms of the Al^{3+}-directed HRP/PAM/Pt/SWCNT/GC electrode in the PBS containing different H_2O_2 concentrations in the absence of oxygen. With the addition of H_2O_2, the reduction peak current of the HRP-Fe(III) dramatically increased, which accompanied by a gradual decrease and even disappearance of the oxidation peak current of the HRP-Fe(II)

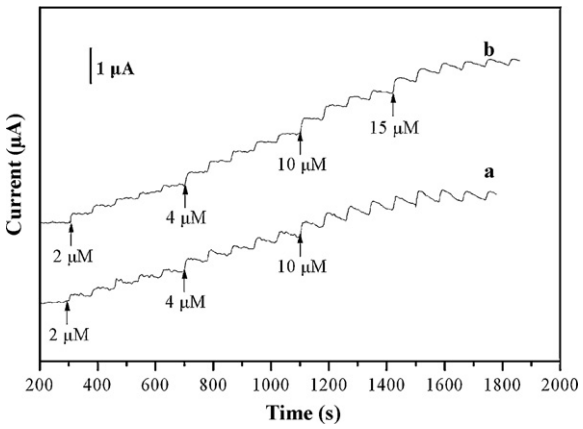

Fig. 6. Typical current-time response curves of the (a) Al^{3+}-directed HRP/PAM and (b) Al^{3+}-directed HRP/PAM/Pt/SWCNT biosensors upon successive addition of H_2O_2 into pH 7.0 PBS. Applied potential: −0.28 V (vs. Ag/AgCl).

(curves b–g), suggesting that an electrocatalytic reduction of H_2O_2 occurred.

As shown in Fig. 5B, the cathodic reduction currents increased linearly with increasing H_2O_2 concentrations and the linear range was from 1.0×10^{-6} to 2.7×10^{-4} M ($R = 0.998$, $n = 21$), which was much wider than those of HRP immobilized on a zirconium-enhanced grafted collagen trihelix scaffold (Zong et al., 2006), a gelatin-hydrophobic ionic liquid gel film (Yan et al., 2007), and a single-crystal CeO_2 nanotube-modified film (Xiao et al., 2009). The lowest detection limit was 0.08 μM at $S/N = 3$, which was rather lower than 1.7 μM at the HRP-toluidine blue-MWCNTs nanocomposite (Liu et al., 2008) and 12.89 μM of HRP based on sol–gel-derived ceramic-carbon nanotube nanocomposite film (Chen and Dong, 2007). The sensitivity of the enzyme electrode was calculated to be about 372 mA cm^{-2} M^{-1}, which was much higher than those of the biosensors constructed with 3D ordered graphitized mesoporous carbon (Lu et al., 2009). This indicated that the biosensor had an excellent bioelectrocatalytic activity towards H_2O_2.

At higher H_2O_2 concentrations, the plot tended to level off, which was characteristic of enzyme-based catalysis. The apparent Michaelis–Menten constant (K_M^{app}) could be estimated according to the Lineweaver–Burk equation (Kamin and Wilson, 1980):

$$I_{ss}^{-1} = I_{max}^{-1} + K_M^{app} C^{-1} I_{max}^{-1}$$

where I_{ss}, I_{max}, and C stand for the steady-state response current after the addition of substrate, the maximum current measured under saturated substrate condition, and the bulk concentration of the substrate, respectively. In this biosensing system, K_M^{app} was estimated to be about 87 μM, which was much smaller than those previously reported (570 and 1760 μM) (Xu et al., 2006; Xiang et al., 2009). The relatively small K_M^{app} indicated that the Al^{3+}-directed HRP/PAM/Pt/SWCNT/GC electrode had high catalytic efficiency to the reduction of H_2O_2.

3.6. Amperometric response of the as-prepared H_2O_2 biosensors

To demonstrate the success of H_2O_2 determination at the as-prepared electrodes, the amperometric response of the fabricated electrodes for H_2O_2 was investigated by amperometric current-time curve method. The electrocatalytic reduction peak potential of H_2O_2 at the as-prepared electrodes in PBS, i.e., −0.28 V, was selected as the constant applied potential for the high sensitivity together with a wide linear range. Fig. 6 demonstrates typical current-time curves of the Al^{3+}-directed HRP/PAM/GC and HRP/PAM/Pt/SWCNT/GC electrodes to successive addition of H_2O_2 in PBS. With each additional aliquot of H_2O_2 to the stirring PBS, the reduction currents rose rapidly and reached a stable plateau. Compared with the response time (about 8.9 s, achieving 95% of the steady-state current) of the Al^{3+}-directed HRP/PAM/GC electrode, the Al^{3+}-directed HRP/PAM/Pt/SWCNT biosensor possessed much faster response (about 4.6 s). Moreover, it can be also referred from Fig. 6 that the Al^{3+}-directed HRP/PAM/Pt/SWCNT biosensor displayed better electrocatalytic properties, such as wider linear range, higher sensitivity, and lower detection limit, in comparison with the Al^{3+}-directed HRP/PAM biosensor. This indicated that the Pt/SWCNTs greatly enhanced the electrocatalytic performance of the Al^{3+}-directed HRP/PAM/Pt/SWCNT/GC electrode. Such a rapid response could be attributed to the fast diffusion of the substrate in the Al^{3+}-directed HRP/PAM/Pt/SWCNT self-assembly composite film.

3.7. Reproducibility and stability of the biosensor

The reproducibility of the biosensor was evaluated at a given concentration in the linear range by cyclic voltammetric measurements. The relative standard deviation (R.S.D.) of the biosensor response to 120 μM H_2O_2 for 7 successive measurements was 2.6%, indicating a good reproducibility. To evaluate electrode-to-electrode reproducibility, six biosensors were prepared under the same and independent conditions. The R.S.D. of the biosensors was 3.4%, indicating a good electrode-to-electrode reproducibility.

The stability of the biosensor was studied by comparing the cyclic voltammetric peak currents of the HRP entrapped in the Al^{3+}-directed PAM/Pt/SWCNT with time intervals of 4 h. The decrease of the cathodic peak current of the biosensor immersed in PBS for 4 h was less than 0.4%, indicating that the biosensor possessed an excellent stability. Moreover, the biosensor could retain 96.0% of its initial response after four-week storage, suggesting a good long-term stability. The good reproducibility and stability can be ascribed to the unique microstructure, shape, and good biocompatibility of the Al^{3+}-directed HRP/PAM/Pt/SWCNT self-assembly film.

4. Conclusion

A novel general methodology for protein immobilization and third-generation biosensor construction, i.e., Al^{3+}-directed PAM self-assembly into ordered 3D dendriform structure, is demonstrated. The dendriform structure easily immobilizes enzymes and nanoparticles. The Al^{3+}-directed PAM/Pt/SWCNT film with ordered 3D structure and highly active sites was explored for the construction of electrochemical biosensor, and has also been proved to be a good matrix for protein immobilization and electrochemical biosensor construction, which may have great impact on the design and application of electrochemical biosensors. With advantages of the Pt/SWCNT heterojunction and porous ordered structures, facilitated direct electron transfer and good biocatalytic activity could be easily obtained through entrapping metalloenzymes into the Al^{3+}-directed PAM/Pt/SWCNT composite material. These results revealed that HRP entrapped in the composite film retained its essential secondary structure and the Al^{3+}-directed HRP/PAM/Pt/SWCNT biosensor displayed good electrochemical performance such as a wide linear range, low detection limit, high sensitivity, good reproducibility and stability, and good long-term stability for the detection of H_2O_2. Comparative experiments demonstrated that the Pt/SWCNT heterojunctions played a decisive role in the formation of the 3D ordered HRP/PAM/Pt/SWCNT film and the enhancement of direct electron transfer capacity and biocatalytic activity of the HRP/PAM/Pt/SWCNT biosensor. The

HRP/PAM/Pt/SWCNT composite film is also expected to find potential applications in biomedical, food, and environmental analysis and detection.

Acknowledgements

The work was supported by National Natural Science Foundation of China (No. 20773040), and The Research Fund for the Doctoral Program (New Young Teacher) of Higher Education (No. 20070561005).

Appendix A. Supplementary data

Supplementary data associated with this article can be found, in the online version, at doi:10.1016/j.bios.2009.10.007.

References

Armstrong, F.A., Hill, H.A.O., Walton, N.J., 1988. Acc. Chem. Res. 21, 407–413.
Arya, S.K., Solanki, P.R., Datta, M., Malhotra, B.D., 2009. Biosens. Bioelectron. 24, 2810–2817.
Bachtold, A., Hadley, P., Nakanishi, T., Dekker, C., 2001. Science 294, 1317–1320.
Cai, W.S., Huang, R.H., 2001. Eur. Polym. J. 37, 1553–1559.
Cao, Z.J., Jiang, X.Q., Xie, Q.J., Yao, S.Z., 2008. Biosens. Bioelectron. 24, 222–227.
Chen, H.J., Dong, S.J., 2007. Biosens. Bioelectron. 22, 1811–1815.
Chen, X.H., Hu, J.Q., Chen, Z.W., Feng, X.M., Li, A.Q., 2009. Biosens. Bioelectron. 24, 3448–3454.
Feng, X.M., Hu, J.Q., Chen, X.H., Xie, J.S., Liu, Y.Y., 2009. J. Phys. D: Appl. Phys. 42, 042001.
Gu, B.X., Xu, C.X., Zhu, G.P., Liu, S.Q., Chen, L.Y., Wang, M.L., Zhu, J.J., 2009. J. Phys. Chem. B 113, 6553–6557.
Heller, A., 1990. Acc. Chem. Res. 23, 128–134.
Huang, H., Hu, N.F., Zeng, Y.H., Zhou, G., 2002. Anal. Biochem. 308, 141–151.
Jia, N.Q., Zhou, Q., Liu, L., Yan, M.M., Jiang, Z.Y., 2005. J. Electroanal. Chem. 580, 213–221.
Kafi, A.K.M., Wu, G.S., Chen, A.C., 2008. Biosens. Bioelectron. 24, 566–571.
Kamin, R.A., Wilson, G.S., 1980. Anal. Chem. 52, 1198–1205.
Laviron, E., 1974. J. Electroanal. Chem. 52, 355–393.
Li, A.Q., Popova-Butler, A., Dean, D.H., Denlinger, D.L., 2007. J. Insect Physiol. 53, 385–391.
Li, H., Zhang, P., Zhang, L., Zhou, T., Hu, D.D., 2009. J. Mater. Chem. 19, 4575–4586.
Lin, Y., Rao, A.M., Sadanadan, B., Kenik, E.A., Sun, Y.P., 2002. J. Phys. Chem. B 106, 1294–1298.
Liu, Y., Lei, J.P., Ju, H.X., 2008. Talanta 74, 965–970.
Lopez, M.S.P., Perez, J.P., Lopez-Cabarcos, E., Lopez-Ruiz, R., 2007. Electroanalysis 19, 370–378.
Lu, X.B., Xiao, Y., Lei, Z.B., Chen, J.P., Zhang, H.J., Ni, Y.W., Zhang, Q., 2009. J. Mater. Chem. 19, 4707–4714.
Montanari, L., Scotti, R., Lockhart, T.P., 1994. Macromolecules 27, 3341–3348.
Murray, R.W., 1984. In: Bard, A.J. (Ed.), Electroanalytical Chemistry. Marcel Dekker, New York, pp. 191–368.
Pal, S., Alocilja, E.C., Downes, F.P., 2007. Biosens. Bioelectron. 22, 2329–2336.
Pei, R.J., Cheng, Z.L., Wang, E.K., Yang, X.R., 2001. Biosens. Bioelectron. 16, 355–361.
Perez, J.P.H., Lopez, M.S.P., Lopez-Cabarcos, E., Lopez-Ruiz, B., 2006. Biosens. Bioelectron. 22, 429–439.
Sanghi, R., Bhattacharya, B., Singh, V., 2006. Bioresour. Technol. 97, 1259–1264.
Sojka, R.E., Bjomeberg, D.L., Entry, J.A., Lentz, R.D., Orts, W.J., 2007. Adv. Agron. 92, 75–162.
Tian, N., Zhou, Z.Y., Sun, S.G., Ding, Y., Wang, Z.L., 2007. Science 316, 732–735.
Varshney, M., Li, Y.B., 2009. Biosens. Bioelectron. 24, 2951–2960.
Wang, Z.J., Li, M.Y., Su, P.P., Zhang, Y.J., Shen, Y.F., Han, D.X., Ivaska, A., Niu, L., 2008. Electrochem. Commun. 10, 306–310.
Wen, Z.H., Wang, Q., Li, J.H., 2008. Adv. Funct. Mater. 18, 959–964.
Xiang, C.L., Zou, Y.J., Sun, L.X., Xu, F., 2009. Sens. Actuators B: Chem. 136, 158–162.
Xiang, J., Lu, W., Hu, Y.J., Wu, Y., Yan, H., Lieber, C.M., 2006. Nature 441, 489–493.
Xiao, X.L., Luan, Q.F., Yao, X., Zhou, K.B., 2009. Biosens. Bioelectron. 24, 2447–2451.
Xu, Q., Mao, C., Liu, N.N., Zhu, J.J., Sheng, J., 2006. Biosens. Bioelectron. 22, 768–773.
Yan, R., Zhao, F.Q., Li, J.W., Mao, F., Fan, S.S., Zeng, B.Z., 2007. Electrochim. Acta 52, 7425–7431.
Zhang, L., Zhang, Q., Li, J.H., 2007. Adv. Funct. Mater. 17, 1958–1965.
Zhao, X.J., Mai, Z.B., Kang, X.H., Zou, X.Y., 2008. Biosens. Bioelectron. 23, 1032–1038.
Zong, S.Z., Cao, Y., Zhou, Y.M., Ju, H.X., 2006. Langmuir 22, 8915–8919.